

Adiabaticity in semiclassical nanoelectromechanical systems

A. Metelmann* and T. Brandes

Institut für Theoretische Physik, TU Berlin, Hardenbergstr. 36, D-10623 Berlin, Germany

(Dated: November 22, 2018)

We compare the semiclassical description of NEMS within and beyond the adiabatic approximation. We consider a NEMS model which contains a single phonon (oscillator) mode linearly coupled to an electronic few-level system in contact with external particle reservoirs (leads). Using Feynman-Vernon influence functional theory, we derive a Langevin equation for the oscillator trajectory that is non-perturbative in the system-leads coupling. A stationary electronic current through the system generates nontrivial dynamical behavior of the oscillator, even in the adiabatic regime. The ‘backaction’ of the oscillator onto the current is studied as well. For the two simplest cases of one and two coupled electronic levels, we discuss the differences between the adiabatic and the non-adiabatic regime of the oscillator dynamics.

PACS numbers: 71.38.-k, 73.21.La, 85.85.+j

I. INTRODUCTION

Nanoelectromechanical systems (NEMS) enable the detailed study of the interaction between electrons, tunneling through a nano-scale device, and the degrees of freedom of a mechanical system. The electronic current affects the mechanical system and vice versa. The dimensions of systems used in recent experiments range down to scales, where the observation of fundamental quantum behavior for a comparatively macroscopic object is possible^{1,2}.

The influence of strong electron-phonon coupling in molecules or suspended quantum dots yields highly interesting effects³⁻⁵, like the Franck-Condon blockade, where the influence of the mechanical system suppresses the electronic current^{3,5}, or switching in molecular junctions⁶.

In non-equilibrium, a standard approach to solve the dynamics of NEMS is to do perturbation theory in a tunnel Hamiltonian, which has been successfully done up to the co-tunneling regime⁷. This is a well-explored path, where the dynamics is described by master equations or generalizations thereof in Liouville space. Many interesting physical results can be obtained via this approach, e.g. avalanche-type molecular transport⁸ or laser-like instabilities⁹. These methods produce good results in the range of high bias, where non-Markovian effects can be neglected. To gain access to the small bias regime, one has to work perturbatively in the system-oscillator instead of the system-leads coupling¹⁰. Alternatively, if the oscillator is treated in a semiclassical regime, Feynman-Vernon influence functional techniques are suitable¹¹⁻¹⁵.

In a previous work, we combined a semiclassical analysis with an adiabatic approach¹⁶, where we assumed the oscillator movement to be slow compared to the electrons which are jumping through the system. The condition $\Gamma \gg \omega_0$ then followed from this approximation, where Γ denotes the tunneling rate of the electrons and ω_0 is the oscillator frequency. The most interesting results, such as negative damping and limit cycles, were achieved in the regime where the oscillator and the electrons act on the

same time scale. But in the latter regime, the adiabatic approach was at the limits of its validity.

In recent publications different approaches, e.g. based on scattering theory^{17,18}, were used to go beyond the adiabatic approximation or to verify the range of validity for this approach^{19,20}. In this paper, we go one step further and present numerical results for a completely non-adiabatic approach. We apply our method to two simple NEMS models, the single and the two-level system. We work in the semiclassical regime where an expansion around the classical path is performed. The advantage of this method is that we are non-perturbative in the system-leads coupling, because the exact electronic solutions are included. In the non-adiabatic approach, we can treat the oscillator and the electrons on the same time scale without further constraints. Therefore, we modify our adiabatic path-integral approach, obtaining an explicit time-dependent perturbation. As a consequence, we have to calculate system quantities numerically in a full time dependent manner. This allows us to critically assess the validity of the adiabatic results. By comparing the outcomes of the adiabatic and the non-adiabatic approach we find a qualitative accordance. The same features arise in both approaches and the stationary results predominantly coincide, but there is no quantitative accordance in the time-dependent regimes. The differences increase together with the complexity of the focused NEMS model.

This paper is organized as follows. In Sec. II we introduce the general model, followed by the derivation of the stochastic equation of motion for the oscillator dynamics. In Sec. III we present the results for a single resonant level system, comparing the adiabatic and the non-adiabatic regime. In addition to the phase space trajectories, we calculate the resulting electronic current through the system. In Sec. IV we consider a two-level system, where the dynamical behavior of the oscillator exhibits non-trivial effects. Thereby we show that the oscillations of the mechanical subsystem lead to an oscillating current with fixed frequency.

II. MODEL

Our total Hamiltonian is a sum of an electronic system \mathcal{H}_e , a single oscillator with a spatial degree of freedom \hat{q} in a harmonic potential \mathcal{H}_{osc} and a linear coupling between the oscillator and the electronic system

$$\mathcal{H} = \mathcal{H}_e + \mathcal{H}_{\text{osc}} - \hat{F}\hat{q}, \quad (1)$$

in which \hat{F} denotes an electronic force operator. The electronic system itself consists of a few electronic levels which are connected to two macroscopic leads. The latter are considered as two Fermi seas with chemical potential $\mu_{\alpha \in \text{L,R}}$ and temperature T . Furthermore, the electronic part provides a non-equilibrium environment for the system. In our formalism we work non-perturbatively in the system-leads coupling, assuming arbitrary coupling and a finite bias regime without constrains.

The single oscillator with momentum \hat{p} , position \hat{q} and mass m is described by a parabolic potential

$$\mathcal{H}_{\text{osc}} = \frac{1}{2m}\hat{p}^2 + \frac{1}{2}m\omega_0^2\hat{q}^2, \quad (2)$$

whereby ω_0 equals the oscillator frequency. The oscillator potential will be modified by the electronic environment and will exhibit multi-stabilities due to the electronic forces¹⁶. In this paper, the reduced Planck constant is set to unity ($\hbar = 1$).

A. Influence functional

We want to focus on the oscillator's dynamics, which is described by the reduced density matrix $\rho_{\text{osc}}(t)$, obtained from the total density matrix $\chi(t)$ by tracing out the bath degrees of freedom, $\rho_{\text{osc}}(t) = \text{tr}_{\text{B}} \chi(t)$. The propagation of the reduced density matrix in time can be written as a double path integral over q_t (forward) and q'_t (backward) weighted by the Feynman-Vernon influence functional^{21,22}

$$\mathcal{F}[q_t; q'_t] = \text{tr}_{\text{B}}(U^\dagger[q'_t] U[q_t]), \quad (3)$$

containing the time evolution operator

$$U[q_t] = T e^{-i \int_0^t dt' [\mathcal{H}_e - \hat{F}q_{t'}]}. \quad (4)$$

The time-ordering operator T arranges operators with later times to the left.

We want to perform an expansion around the classical path. Therefore we transform to center-of-mass and relative path variables

$$q_t = x_t + \frac{1}{2}y_t, \quad q'_t = x_t - \frac{1}{2}y_t, \quad (5)$$

where the variable y_t can be interpreted as the quantum fluctuations around the classical path. We introduce an

interaction picture

$$\begin{aligned} U[q_t] &= T e^{-i \int_0^t dt' [\hat{H}_e - \hat{F}x_{t'} - \frac{1}{2}\hat{F}y_{t'}]} \\ &= U[x_t] \tilde{U}[y_t]; \quad \tilde{U}[y_t] = T e^{i \int_0^t dt' \frac{1}{2}\tilde{F}(t')y_{t'}}, \end{aligned} \quad (6)$$

where the term with the off-diagonal path y_t is regarded as a perturbation and $\tilde{F}(t) = U^\dagger[x_t] \hat{F} U[x_t]$. Inserting Eq. (6) into the influence functional, Eq. (3), leads to

$$\begin{aligned} \mathcal{F}[q_t; q'_t] &= \text{tr}_{\text{B}}(\tilde{U}^\dagger[-y_t] U^\dagger[x_t] U[x_t] \tilde{U}[y_t]) \\ &= \text{tr}_{\text{B}}(\tilde{U}^\dagger[-y_t] \tilde{U}[y_t]). \end{aligned} \quad (7)$$

Expanding this term to second order and performing a cluster expansion²³, we finally obtain

$$\mathcal{F}^{\text{pert}}[q_t; q'_t] = e^{-\Phi[x_t; y_t]}, \quad (8)$$

with the influence phase

$$\Phi[x_t; y_t] = -i \int_0^t dt' f(t')y_{t'} + \int_0^t dt' \int_0^t ds C(t', s)y_{t'}y_s, \quad (9)$$

and the force correlation function

$$\begin{aligned} C(t', s) &= \text{tr}_{\text{B}} \left\{ \left(\tilde{F}(t') - f(t') \right) \left(\tilde{F}(s) - f(s) \right) \right\} \\ &\equiv \langle \delta \tilde{F}(t') \delta \tilde{F}(s) \rangle. \end{aligned} \quad (10)$$

The force term $f(t) \equiv \langle \tilde{F}(t) \rangle$ depends on the center of mass path x_t . The influence phase, Eq. (9), can be regarded as a cumulant generating functional for the force operator correlation functions. The term of quadratic order in y_t describes the Gaussian fluctuations around the classical trajectory which is determined self-consistently in our approach. Higher order terms in y_t (corresponding to non-Gaussian noise) describe higher quantum fluctuations which are neglected here.

B. Langevin equation

To second order in y_t the double path integral for the reduced density matrix describes a classical stochastic process for the diagonal path x_t that is defined by a (non-adiabatic) Langevin equation

$$m\ddot{x}_t + V'_{\text{osc}}(x_t) - f[x_t] = \xi_t \quad (11)$$

with $V'_{\text{osc}}(x_t) = m\omega_0^2 x_t$ and a Gaussian stochastic force ξ_t that has a correlation function $\langle \xi_{t'} \xi_s \rangle = C(t', s)$. Eq. (11) is the starting point for our non-adiabatic calculations. Note that the force $f[x_t]$ is a complicated functional that contains the full time-dependence of the position operator x_t .

In the adiabatic approximation, a Taylor expansion for the center of mass variable is performed ($x_t \approx x_0 + t \cdot \dot{x}_0$),

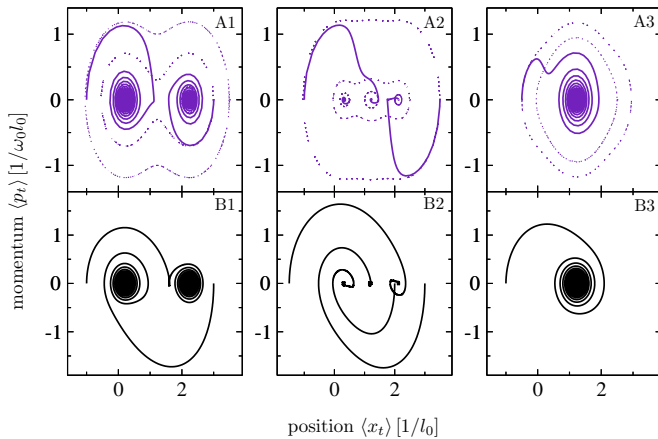


FIG. 1: Phase space portraits resulting from the (non-) adiabatic approach in units of ω_0 and l_0 with the parameters $\Gamma = 1.4\omega_0$, $\varepsilon_d = 3.0\omega_0$ and $g = 2.45$ at zero temperature. Row A depicts the adiabatic results, additionally the case without friction is plotted (dotted lines). Row (B) depicts the non-adiabatic results. The bias voltage (symmetric choice) is increased from left to right, explicit values are $V_{\text{bias}}/\omega_0 = 0.5/2.5/5.0$.

leading to an interaction picture with respect to $\mathcal{H}_0 = \mathcal{H}_e - \hat{F}x_0$ and a perturbation $V[q](t) = -\hat{F}(t\hat{x}_0 + \frac{1}{2}y_t)$. Consequently, the expectation value of the force operator in the adiabatic interaction picture can be calculated for fixed x_0 . Additionally, due to the second term $t\hat{x}_0$ of the Taylor expansion, an explicit friction term arises in the (adiabatic) Langevin equation,

$$m\ddot{x}_t + V'_{\text{osc}}(x_t) + \dot{x}_t D[x_t] - \tilde{f}[x_t] = \xi_t. \quad (12)$$

The friction term $D[x_t]$ can be interpreted as the first adiabatic correction term.

In contrast, in the non-adiabatic Eq. (11), all higher orders of the Taylor expansion are included and the first challenge is to calculate the force term $f[x_t]$ considering the full time-dependence of x_t . In all our calculations presented in this paper we neglect the stochastic fluctuations ($\xi_t = 0$).

III. SINGLE RESONANT LEVEL

The Hamiltonian for the single resonant level (Anderson-Holstein model – AHM) is

$$\mathcal{H} = \sum_{k\alpha} \varepsilon_{k\alpha} \hat{c}_{k\alpha}^\dagger \hat{c}_{k\alpha} + \sum_{k\alpha} \left(V_{k\alpha} \hat{c}_{k\alpha}^\dagger \hat{d} + h.c. \right) + \varepsilon \hat{d}^\dagger \hat{d} + \mathcal{H}_{\text{osc}}, \quad (13)$$

with the abbreviation $\varepsilon = \varepsilon_d - \lambda\hat{q}$, containing the energy of the local level ε_d and the linear coupling to the oscillator. Thereby, λ equates the coupling strength. The operators \hat{d}/\hat{d}^\dagger correspond to the dot, and the lead operators $\hat{c}_{k\alpha}/\hat{c}_{k\alpha}^\dagger$ annihilate/create an electron in the α -lead with energy $\varepsilon_{k\alpha}$ and momentum k , whereby $\alpha = \text{L, R}$ denote the left/right lead. Transitions of electrons between

the dot and the α -lead are possible with the amplitude $V_{k\alpha}$. Here, the force operator becomes $\hat{F} = \lambda\hat{d}^\dagger \hat{d} = \lambda\hat{n}_d$ and the self-consistent equation of motion for the expectation value of the oscillator coordinate x_t (neglecting stochastic fluctuations) reads

$$\begin{aligned} m\ddot{x}_t + V'_{\text{osc}}(x_t) - \lambda N[x_t] &= 0 \\ N[x_t] &\equiv \text{tr}_{\text{B}}(U^\dagger[x_t] \hat{n}_d U[x_t]). \end{aligned} \quad (14)$$

The occupation number of the local level $N[x_t]$ is calculated with the lesser Green function

$$N[x_t] = \langle \tilde{d}^\dagger(t) \tilde{d}(t) \rangle = -iG^<(t, t), \quad (15)$$

which is obtained from the Keldysh equation

$$G^<(t, t) = \int dt_1 \int dt_2 G^r(t, t_1) \Sigma^<(t_1, t_2) G^a(t_2, t), \quad (16)$$

containing the advanced/retarded Green function

$$G^{r,a}(t, t') = \mp i \Theta(\pm t \mp t') e^{-i \int_{t'}^t dt'' [\varepsilon(t'') \mp i \frac{\Gamma}{2}]}, \quad (17)$$

with $\varepsilon(t) \equiv \varepsilon_d - \lambda x_t$. Thereby, Θ designates the Heaviside step function. In the time dependent case the lesser self energy²⁴ reads

$$\Sigma^<(t_1, t_2) = i \sum_{\alpha \in \text{L, R}} \int \frac{d\omega}{2\pi} e^{-i\omega(t_1 - t_2)} f_\alpha(\omega) \Gamma_\alpha, \quad (18)$$

whereby $f_\alpha(\omega)$ denotes the Fermi function. We assume constant tunneling rates $\Gamma_\alpha = 2\pi \sum_k |V_{k\alpha}|^2 \delta(\omega - \varepsilon_{k\alpha}) = \Gamma/2$, i.e. the left and the right tunneling rate are equal with $\Gamma \equiv \Gamma_{\text{L}} + \Gamma_{\text{R}}$. As a result, for the time dependent occupation we obtain

$$N[x_t] = \sum_{\alpha \in \text{L, R}} \Gamma_\alpha \int \frac{d\omega}{2\pi} f_\alpha(\omega) |A(\omega, t)|^2, \quad (19)$$

with the spectral function

$$A(\omega, t) = -i \int_{t_0}^t dt' e^{-i \int_{t'}^t dt'' (\varepsilon(t'') - \omega - i \frac{\Gamma}{2})}. \quad (20)$$

To solve the equation of motion without any further approximation and expansion, we transform Eq. (20) into the differential equation

$$\dot{A}(\omega, t) = -i - i \left(\varepsilon_d - \lambda x_t - \omega - i \frac{\Gamma}{2} \right) A(\omega, t). \quad (21)$$

For the numerical integration a trapezoidal rule for discrete functions is applied. Thus we solve Eq. (21) to-

gether with the system

$$\begin{aligned} \dot{x}_t &= \frac{1}{m} p_t \\ \dot{p}_t &= -V'_{\text{osc}} + \lambda \sum_{\alpha \in \text{L,R}} \frac{\Gamma_{\alpha}}{4\pi} \Delta\omega \\ &\quad \sum_{n=0}^{N-1} [f_{\alpha}(\omega_{n+1}) |A(\omega_{n+1}, t)|^2 + f_{\alpha}(\omega_n) |A(\omega_n, t)|^2] \end{aligned} \quad (22)$$

with $\Delta\omega = |\omega_N - \omega_0|/N$, in which N equals the number of points of the discretization scheme.

Figure 1 depicts the results in the oscillator phase space for different bias values. All data are obtained for a small tunneling rate $\Gamma = 1.4\omega_0$, close to the limit of validity of the adiabatic approach which requires $\Gamma \gg \omega_0$. In order to obtain correct physical units we introduce the dimensionless coupling parameter $g = \lambda/(m\omega_0^2 l_0)$, whereby $l_0 \equiv 1/\sqrt{m\omega_0}$ equals the oscillator length. Row A shows the adiabatic results. The dotted lines correspond to the adiabatic case without the first adiabatic correction term. Here, the trajectories run about the fixed points of the system. By varying the applied bias, the number of fixed points changes and in the case of high bias only one fixed point survives. Turning on the friction (first adiabatic correction term) leads to the solid line results in the graphs of row A. Here, the centers turn into stable spirals and the trajectories end up in the fixed points. (For further explanation see¹⁶). In row B the non-adiabatic results are depicted. After long times t we observe little variation to the adiabatic result, nevertheless all trajectories end up in the same fixed points. By comparing both approaches the largest differences emerge for small times. This qualitative good accordance can also be observed in the results for the electronic current. In the non-adiabatic approach, the current is obtained from²⁴

$$\mathcal{I}_{\alpha}(t) = -e\Gamma_{\alpha} \left[N [x_t] + \int \frac{d\omega}{\pi} f_{\alpha}(\omega) \text{Im} [A(\omega, t)] \right]. \quad (23)$$

The imaginary part of the spectral function is negative and describes the current flowing from the left lead into the dot. While keeping the oscillator center of mass coordinate $x_t \equiv x$ fixed in Eq. (23) when calculating the spectral function, the adiabatic current result is reproduced. Starting from Eq. (20) we obtain

$$A^{\text{adiabatic}}(\omega, t) = \frac{e^{-i(\varepsilon_d - \lambda x - \omega - i\frac{\Gamma}{2})(t-t_0)} - 1}{(\varepsilon_d - \lambda x - \omega - i\frac{\Gamma}{2})}. \quad (24)$$

For large times $t - t_0$, the first exponential can be neglected and the spectral function becomes stationary. Therefore the adiabatic current reads (zero temperature)

$$\mathcal{I}_L = e \frac{\Gamma}{4\pi} \left[\arctan \frac{2(\mu_L - \varepsilon_d + \lambda x)}{\Gamma} - \arctan \frac{2(\mu_R - \varepsilon_d + \lambda x)}{\Gamma} \right] = -\mathcal{I}_R. \quad (25)$$

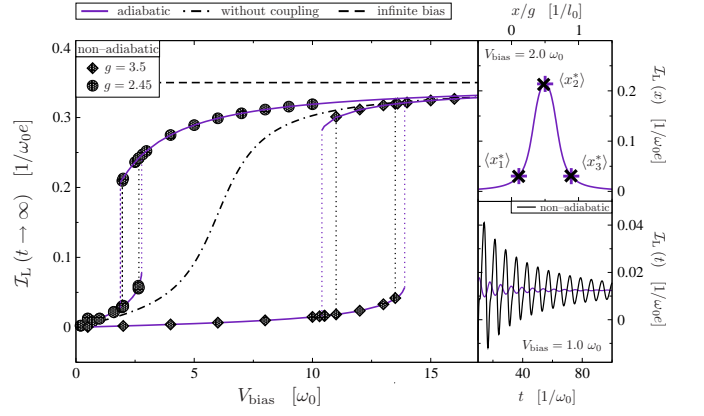


FIG. 2: LEFT: Current for $t \rightarrow \infty$ as a function of V_{bias} for two different coupling parameters g and with $\Gamma = 1.4\omega_0$, $\varepsilon_d = 3.0\omega_0$ at zero temperature. The black symbols depict the non-adiabatic and the indigo solid line the adiabatic results. For comparison the infinite bias result (dashed line) and the current without coupling (dashed-dotted line) are plotted. The dotted lines mark the hysteresis like regimes, where two clearly distinct current channels exist. RIGHT: The upper graph depicts the position dependent current $\mathcal{I}_L(x)$ for $V_{\text{bias}} = 2.0\omega_0$, the three fixed points are marked as crosses. The lower graph shows the left current for small times and $V_{\text{bias}} = 1.0\omega_0$. Remaining parameters are equal to the left graph and $g = 2.45$.

This is a well known result and for the infinite bias case we obtain $\mathcal{I}_{L,R}^{\text{IB}} = \pm e\Gamma/4$ as expected. Note, that in the adiabatic case the values for left and right current only differ in their sign.

In the left graph of Figure 2 the stationary left current $\mathcal{I}_L(t \rightarrow \infty)$ is depicted for increasing bias and for two different coupling parameters g . As explained above, the oscillator trajectories end up in fixed points for large times. Hence, the current $\mathcal{I}_L(t \rightarrow \infty)$ becomes stationary and its value corresponds to a single level which is shifted by $-gx^*/l_0$, whereby x^* corresponds to a fixed point. Because the system owns multiple fixed points, we obtain several current channels depending on the initial condition. The dashed-dotted line in Figure 2 corresponds to the case without coupling to the oscillator ($g = 0$). For small bias, the current is small compared to the infinite bias case (dashed line). There, the effective level $\tilde{\varepsilon} = \varepsilon_d - gx^*/l_0$ is situated outside the transport window. The latter is also valid for the case without coupling, due to $\tilde{\varepsilon} = \varepsilon_d = 3.0\omega_0$. The bias range for the current suppression is larger in the case of stronger coupling to the oscillator ($g = 3.5$). We obtain a hysteresis like shape for the current evolution, which is due to the multi-stability of the system. The coupling between the electronic and the mechanical system leads to a modified oscillator potential with additional minima. Switching between these states is possible and was theoretical proposed and studied by several authors^{13,25,26}.

The beginning and the ending of the hysteresis regime, where two current channels exist, are denoted by vertical

dotted lines in Figure 2. For the non-adiabatic case the latter regime, where two current channels exist, differs a bit from the adiabatic case.

The upper right graph of Figure 2 shows the current $\mathcal{I}_L(x)$ for the bias value $V_{\text{bias}} = 2.0\omega_0$. Here, three fixed points occur, denoted by a cross. For $\langle x_2^* \rangle \approx g/2l_0$ the effective level is situated in the middle of the transport window and following from that the current is maximal. For the two other fixed points the effective level is again situated outside the transport window and the current is small.

By comparing the adiabatic and the non-adiabatic stationary currents, we can conclude that in the long-time limit only small differences exist. The differences are at their maximum for small times, which is clearly visible in the lower right graph of Figure 2, which depicts $\mathcal{I}_L(t)$. There, the oscillations in the non-adiabatic case are much larger.

The left and right time dependent currents differ for small times t in the non-adiabatic case. When we integrate \mathcal{I}_L and \mathcal{I}_R over all times the results coincide, so that there is no violation of current conservation. This is comparable to a periodically driven system with time dependent tunneling rates²⁷. The spectral function defined in Eq. (20), is sensitive to small time differences $t - t_0$. For larger times the oscillator settles into one of the fixed points, whereas the spectral function becomes stationary and hence also the current.

IV. TWO-LEVEL SYSTEM

The model we are treating in this section consists of two single dot levels which are coupled by a tunnel barrier. Again we assume a coupling to a single bosonic mode. The total Hamiltonian is composed of the oscillator part \mathcal{H}_{osc} , cf. Eq. (2), the electronic part \mathcal{H}_e and an interaction part which describes the coupling between the oscillator and the two dots. In contrast to the AHM, here the oscillator couples to the difference of the occupation numbers with the coupling strength λ . The total Hamiltonian therefore reads

$$\mathcal{H} = \mathcal{H}_e + \mathcal{H}_{\text{osc}} - \lambda \hat{q} (\hat{d}_L^\dagger \hat{d}_L - \hat{d}_R^\dagger \hat{d}_R), \quad (26)$$

containing the electronic part

$$\begin{aligned} \mathcal{H}_e = & \sum_{k\alpha} \varepsilon_{k\alpha} c_{k\alpha}^\dagger c_{k\alpha} + \sum_{k\alpha} V_{k\alpha} c_{k\alpha}^\dagger d_\alpha + V_{k\alpha}^* d_\alpha^\dagger c_{k\alpha} \\ & + \sum_\alpha \nu_\alpha d_\alpha^\dagger d_\alpha + T_c d_L^\dagger d_R + T_c^* d_R^\dagger d_L, \end{aligned} \quad (27)$$

where $\nu_{\alpha \in L,R}$ denotes the left and right dot energy levels. Here, T_c denotes the tunnel coupling matrix element between the two dots. Again, we obtain a Langevin equation, Eq. (11), with the force term

$$f[x_t] = \lambda \langle \sigma_z \rangle(t) \equiv \lambda [\langle n_L \rangle(t) - \langle n_R \rangle(t)], \quad (28)$$

where $\langle n_{L/R} \rangle(t)$ implicitly depend on the oscillator coordinate x_t , cf. below.

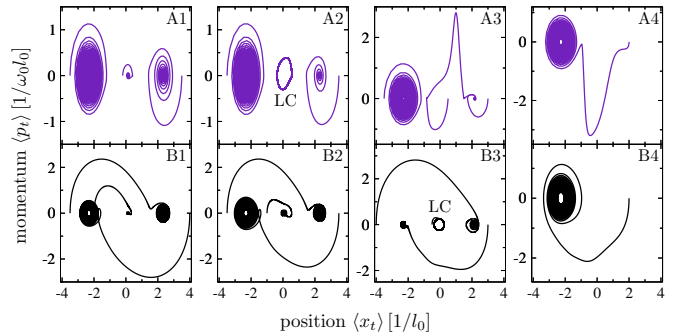


FIG. 3: Phase space portraits for various tunnel couplings T_c , increasing from left to right. Upper row A: adiabatic results. Lower row B: non-adiabatic results. In graphs A2 and B3 limit cycles (LC) appear. Explicit parameters are $|T_c|^2 = 0.2; 0.4; 1.0; 4.0 \omega_0^2$. With the rate $\Gamma = 2.0\omega_0$ and for the chemical potentials we assumed $\mu_L = \omega_0$ and $\mu_R = -5\omega_0$. The dimensionless coupling constant is chosen as $g = 2.5$, and the internal bias voltage as $V_{\text{int}} = 5\omega_0$, whereas $\nu_L = -\nu_R = eV_{\text{int}}/2$.

A. Time dependent occupation

Calculating the time dependent occupations for the two level system using Green's functions is a challenge due to the complex dependencies and couplings of the systems operators. We choose a more direct way by using the equations of motion technique, leading to a large system of coupled differential equations which have to be solved numerically.

The Heisenberg equations of motion for operators of the dots and the leads ($\tilde{\nu}_\alpha(t) = \nu_\alpha \mp \lambda x_t$) yield

$$\begin{aligned} \dot{\tilde{d}}_L(t) = & -i \left(\tilde{\nu}_L(t) - i\frac{\Gamma}{4} \right) \tilde{d}_L(t) - iT_c^* \tilde{d}_R(t) + \sum_k \tilde{C}_{kL}(t), \\ \dot{\tilde{d}}_R(t) = & -i \left(\tilde{\nu}_R(t) - i\frac{\Gamma}{4} \right) \tilde{d}_R(t) - iT_c \tilde{d}_L(t) + \sum_k \tilde{C}_{kR}(t), \end{aligned} \quad (29)$$

where $\tilde{C}_{k\alpha}(t) = -iV_{k\alpha}^* e^{-i\varepsilon_{k\alpha}t} \tilde{c}_{k\alpha}(0)$ and the tunneling rate equals $\Gamma_\alpha \equiv 2\pi \sum_k |V_{k\alpha}|^2 \delta(\omega - \varepsilon_{k\alpha})$. Again, we assume constant tunneling rates $\Gamma_L = \Gamma_R = \Gamma/2$.

The equations (29) already include the solution for the inhomogeneous differential equation for the lead operator $\tilde{c}_{k\alpha}$. The tilde denotes the interaction picture introduced above, cf. Eq. (6). Hence, the effective time dependent energy level $\tilde{\nu}_\alpha(t)$ contains only the classical variable x_t .

The differential equations for the corresponding dot annihilation operators are derived in a similar manner. Finally, one obtains an inhomogeneous system of coupled differential equations with time dependent coefficients. Multiplication with $\delta(\omega - \varepsilon_{k,\alpha})$ and summing over all k

states leads to

$$\begin{aligned}
\langle \dot{\tilde{\sigma}}_z \rangle(t) &= -\frac{\Gamma}{2} \langle \tilde{\sigma}_z \rangle(t) + 2 \operatorname{Re} \left[2 D_{RL}(t) \right. \\
&\quad \left. + \int d\omega B_{LL}(\omega, t) - \int d\omega' B_{RR}(\omega', t) \right] \\
\dot{D}_{RL}(t) &= i \left(\tilde{\nu}_R(t) - \tilde{\nu}_L(t) + i \frac{\Gamma}{2} \right) D_{RL}(t) - |T_c|^2 \langle \tilde{\sigma}_z \rangle(t) \\
&\quad + \int d\omega' B_{RL}(\omega', t) - \int d\omega B_{LR}^\dagger(\omega, t) \\
\dot{B}_{\alpha,\alpha}(\omega, t) &= -i \left(\tilde{\nu}_\alpha(t) - \omega - i \frac{\Gamma}{4} \right) B_{\alpha,\alpha}(\omega, t) \\
&\quad - B_{\alpha,\beta}(\omega, t) + \frac{\Gamma}{4\pi} f_\alpha(\omega) \\
\dot{B}_{\alpha,\beta}(\omega, t) &= -i \left(\tilde{\nu}_\beta(t) - \omega - i \frac{\Gamma}{4} \right) B_{\alpha,\beta}(\omega, t) \\
&\quad + |T_c|^2 B_{\alpha,\alpha}(\omega, t), \quad \alpha \neq \beta,
\end{aligned} \tag{30}$$

with the definitions:

$$\begin{aligned}
B_{\alpha\alpha}(\omega, t) &= i V_{k\alpha} \delta(\omega - \varepsilon_{k\alpha}) e^{i\varepsilon_{k\alpha}t} \langle \tilde{c}_{k\alpha}^\dagger(0) \tilde{d}_\alpha(t) \rangle \\
B_{RL}(\omega, t) &= -T_c V_{kR} \delta(\omega - \varepsilon_{kR}) e^{i\varepsilon_{kR}t} \langle \tilde{c}_{kR}^\dagger(0) \tilde{d}_L(t) \rangle \\
B_{LR}(\omega, t) &= -T_c^* V_{kL} \delta(\omega - \varepsilon_{kL}) e^{i\varepsilon_{kL}t} \langle \tilde{c}_{kL}^\dagger(0) \tilde{d}_R(t) \rangle \\
D_{RL}(\omega, t) &= iT_c \langle \tilde{d}_R^\dagger(t) \tilde{d}_L(t) \rangle.
\end{aligned} \tag{31}$$

The system Eq. (30) is solved numerically together with the equations of motion for the expectation values for position and momentum operator

$$\begin{aligned}
\dot{x}_t &= \frac{1}{m} p_t \\
\dot{p}_t &= -V'_{\text{osc}} + \lambda \langle \tilde{\sigma}_z \rangle(t).
\end{aligned} \tag{32}$$

Hence, the phase space trajectories are obtained.

In Figure 3 results for $\Gamma = 2\omega_0$ are plotted. The upper row depicts the result for the adiabatic case including the first correction term. This so-called intrinsic friction term $D[x_t]$, cf. Eq. (12), results from the non-equilibrium electronic environment. The tunnel coupling $|T_c|^2$ increases from left to right. Three fixed points appear in the range of small tunnel coupling (A1). There, the trajectories form stable spirals and run into the fixed points. For $|T_c|^2 = 0.4\omega_0^2$ a limit cycle appears in the middle (A2). By further increasing $|T_c|^2$ the limit cycle turns into an unstable spiral (A3) and in the end only the left fixed points survives (A4).

The second row (B) shows the results for the non-adiabatic approach. Qualitatively the same features emerge, as the appearance of the limit cycle and the stable spirals. Comparing the adiabatic and the non-adiabatic approach, we obtain quantitative differences, like the change of the middle fixed point into a limit cycle which happens at higher values of $|T_c|^2$ as in the adiabatic case. The results differ most for small times, similar to the single level case (Sec.III). By further decreasing the tunneling rate Γ the differences between the

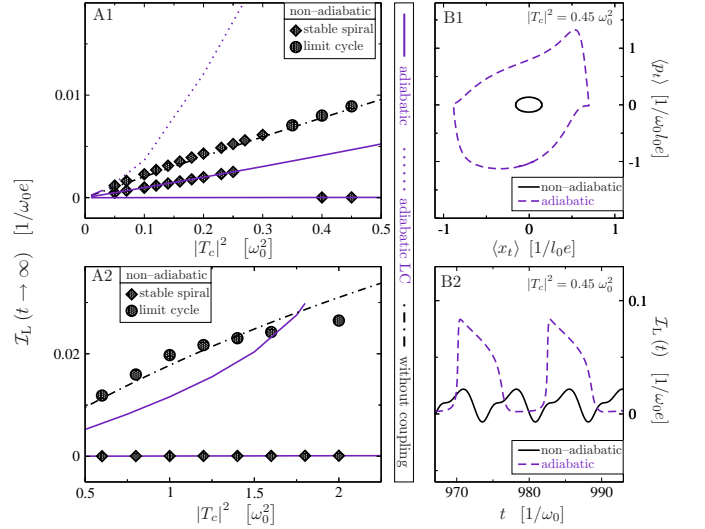


FIG. 4: LEFT: Current for $t \rightarrow \infty$ as a function of tunnel coupling $|T_c|^2$. A1 displays the results for $|T_c|^2 \leq 0.5\omega_0^2$ and A2 the results in the range of $0.5 \leq |T_c|^2/\omega_0^2 \leq 2.0$. The symbols denote the non-adiabatic results. The diamonds correspond to the stable spiral situations, there the oscillation of the dynamical system disappears in the long-time limit and the current becomes stationary. Circles denote averaged current values for the limit cycle case, when the system performs periodic oscillations. The indigo solid (dotted) lines depict the adiabatic results for the stable spiral (limit cycle) case. The dashed-dotted line depicts the current without coupling. RIGHT: The graph B1 shows the phase space results for $|T_c|^2 = 0.45\omega_0^2$, here the radius for the adiabatic limit cycle is much larger than in the non-adiabatic case. Below, graph B2, depicts the corresponding time dependent left current, which oscillates as well. Explicit parameters are $\Gamma = \omega_0$, $\mu_L = \omega_0$ and $\mu_R = -5\omega_0$. The dimensionless coupling constant is chosen as $g = 2.5$, and the internal bias voltage as $V_{\text{int}} = 5\omega_0$, whereas $\nu_L = -\nu_R = eV_{\text{int}}/2$.

approaches increase. Results for a smaller tunneling rate will be presented in the next section, Sec. IV B, there we calculate the electronic current for $\Gamma = \omega_0$.

We also mention that the appearance of the limit cycle in this system is possible due to energy transfer processes between the electrons and the oscillator. In the stable spiral case, the influence of the electrons leads to damping of the oscillator. For example for $\tilde{\nu}_L < \tilde{\nu}_R$, the electrons need energy to pass through the system.

The requirements for a damped dynamical system to exhibit limit cycles is the additional appearance of positive friction. For our system this means, that energy transfer processes occur which lead to the acceleration of the oscillator. The occurrence of positive friction is possible when $\tilde{\nu}_L > \tilde{\nu}_R$ and the electrons can transfer energy to the oscillator, cf. ¹⁶.

B. Current

The current through lead α is derived via the Heisenberg equations of motion and yields

$$\mathcal{I}_\alpha(t) = -e \left[\Gamma_\alpha N_\alpha [x_t] - \int d\omega \text{Re} [B_{\alpha\alpha}(\omega, t)] \right]. \quad (33)$$

The left graphs of Figure 4 depict the stationary current $\mathcal{I}_L(t \rightarrow \infty)$ as a function of the tunnel coupling $|T_c|^2$. In the adiabatic case and for small values of $|T_c|^2$ (A1) we observe two fixed points and one limit cycle leading to a tri-stable current. In the limit cycle case the current oscillates in time. The corresponding averaged current (dotted line) is not completely shown in (A1), due to the large values, since the current increases further until $|T_c|^2 = 0.48\omega_0^2$. There, the limit cycle disappears and two fixed points remain until $|T_c|^2 = 1.8\omega_0^2$ (A2). We also obtain two fixed points in the small range of $|T_c|^2 \leq 0.03\omega_0^2$, which is not dissolved in graph A1 of Figure 4.

The current corresponding to the fixed point $x_* \simeq 2/l_0$ (solid line below $g = 0$ case) increases approximately in the same fashion as in the case without coupling. In this regime the left effective level lays inside the transport window ($\tilde{\nu}_{L,R} \simeq \mp 2.5\omega_0$). For large tunnel coupling one fixed point persists, $x_* \simeq -2.3/l_0$, and the corresponding current (lowest solid line) is strongly suppressed compared to the case without coupling. There, both effective levels $\tilde{\nu}_{L,R} \simeq \pm 7.5\omega_0$ are clearly situated outside the transport window. Therefore tunneling through the two level system is rarely possible.

In the left graphs of Figure 4 the symbols denote the non-adiabatic current in the long-time limit. Here, the system has also two fixed points, but the limit cycle range is much larger, $0.35 \leq |T_c|^2/\omega_0^2 \leq 6.5$. For $|T_c|^2 \leq 0.35\omega_0^2$ we observe two stable fixed points and by increasing the tunnel coupling the middle stable spiral turns into a limit cycle and the mechanical system performs periodic oscillations. For the latter case, the circles in Figure 4 denote the averaged current.

The non-adiabatic current corresponding to the middle fixed point/limit cycle follows the result without coupling. As long as the fixed point $x^* \simeq 0.03/l_0$ is stable the resulting effective level is approximately $\tilde{\nu}_{L,R} \simeq \nu_{L,R}$ as in the case without coupling. In graph B1 of Figure 4, the phase space trajectories are plotted for the case when the system performs periodic oscillations. The limit cycle, corresponding to the non-adiabatic results, runs in small cycles about the origin and following from that, the averaged current is similar to the case without coupling. In the adiabatic case the radius is much larger and the shape of the limit cycle is not smoothly circular. Hence, the current is much larger then in the non-adiabatic case (A1). In graph B2 the related time dependent current is depicted. Frequency and amplitude differ strongly in both cases. The frequency of the current oscillations is equal to the oscillator frequency (non-adiabatic: $\omega \approx 0.86\omega_0$).

The current reaches its maximum when the the distance between the left (right) effective level and the left (right)

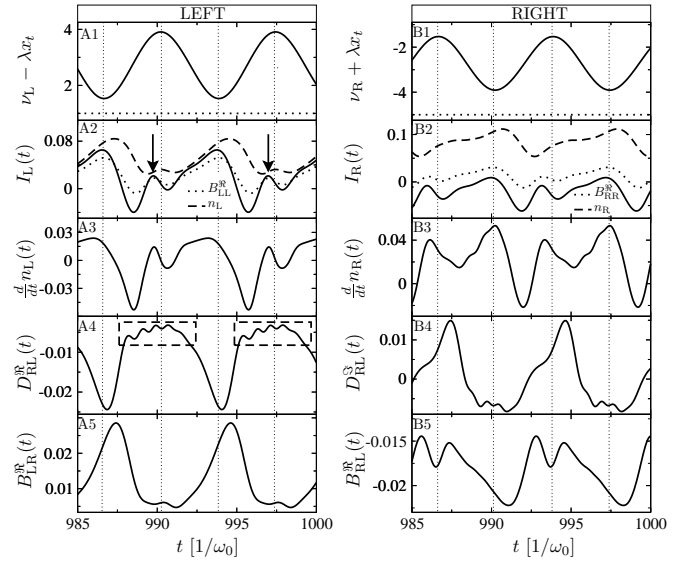


FIG. 5: Time evolution for the current and the corresponding correlation functions for $|T_c|^2 = \omega_0$ in the non-adiabatic limit cycle case. The vertical dotted lines correspond to the maxima/minima of the effective level $\tilde{\nu}_\alpha = \nu_\alpha \mp gx_t/l_0$. The first row depicts the position for the effective left (A1) and right (B1) level and the dotted line corresponds to the chemical potentials $\mu_L = \omega_0$ and $\mu_R = -5\omega_0$. The results for the left/right current are plotted in graph A2/B2, together with the occupation for the left/right level and the real part of the correlation function $B_{LL/RR}$. The time derivative of the level occupation is depicted in row three. Row 4 shows the result for the real (A4) and the imaginary (B4) part of the dot-dot-correlation function D_{RL} . The real parts of $B_{LR/RL}$ are depicted in row 5. The dimensionless coupling constant is chosen as $g = 2.5$, and the internal bias voltage as $V_{\text{int}} = 5\omega_0$, whereas $\nu_L = -\nu_R = eV_{\text{int}}/2$.

chemical potential is minimal (maximal). This is clearly visible in Figure 5, where the time evolution for current and the different correlation functions defined above, cf. Eq. (31), are depicted. The first row shows the behavior of the oscillating effective levels, the value of the chemical potential is also plotted in these graphs (dotted line). In the first graph of the second row the current for the left lead is maximal when the effective level is minimal as mentioned above. The current decreases when the left level increases its distance to the transport window.

The additional current peak (arrows in A2 of Fig. 5) near the maximum of the left effective level does not appear in an adiabatic approach, where the current follows the position of the levels. This peak is related to internal coherent electronic oscillations between the two dots. These oscillations are visible in the real part of the D_{RL} function depicted in graph A4 of Figure 5 (denoted by dashed boxes), with frequencies that match the time dependent Rabi frequency $\omega_R(t) = \sqrt{\tilde{\nu}_L(t) - \tilde{\nu}_R(t) + 4|T_c|^2}$.

In the adiabatic case, the time-resolved current for the right lead is equal to the current through the left lead

with opposite sign. For the non-adiabatic case, right and left time-resolved currents are different, but their time-averages coincide. If we are in the long-time limit, and the system performs no oscillations, left and right current are equal. In contrast, in the limit cycle case we obtain a driven system leading to currents $\bar{I}_{L,R}$ whose time dependence differ, since charge temporarily accumulates in the dots.

V. CONCLUSION

By comparing the adiabatic and non-adiabatic results for the single-level system we obtain a good qualitative agreement. In principle, the same features arise, as bistability and a hysteresis-like $\mathcal{I} - V$ characteristic are ob-

served in both cases. The largest deviations are observed for small times, but in the long time limit the results predominantly coincide.

For the two-level case the differences are much larger. Qualitatively we observe similar properties, but the quantitative predictions of the adiabatic approach do not match the results for the non-adiabatic system where the oscillator and the electrons act on the same timescale. The electron-oscillator interaction leads to multiple current channels like in the single-level system. Additionally, we observe limit cycles of the dynamical system leading to periodic oscillations of the current. In this regime, the system acts as a DC-AC-transformer.

Acknowledgments. This work was supported by projects DFG BR 1528/7-1, DFG BR 1528/8-1 and the Rosa Luxemburg foundation.

-
- * metelmann@itp.tu-berlin.de
- ¹ A. D. O’Connell, M. Hofheinz, M. Ansmann, R. C. Bialczak, M. Lenander, E. Lucero, M. Neeley, D. Sank, H. Wang, M. Weides, J. Wenner, J. M. Martinis and A. N. Cleland, *Nature* **464**, 697 (2010).
 - ² J.D. Teufel, D. Li, M.S. Allman, K. Cicak, A.J. Sirois, J.D. Whittaker, and R.W. Simmonds, *Nature* **471**, 7337 (2011).
 - ³ R. Leturcq, C. Stampfer, K. Inderbitzin, L. Durrer, C. Hierold, E. Mariani, M. G. Schultz, and F. von Oppen, *Nat Phys* **5**, 327 (2009).
 - ⁴ B. Lassange, Y. Tarakanov, J. Kiranet, D. Garcia-Sanchez and A. Bachthold, *Science* **325**, 1107 (2009).
 - ⁵ S. Sapmaz, P. Jarillo-Herrero, Ya. M. Blanter, C. Dekker and H. S. J. van der Zant, *Phys. Rev. Lett.* **96**, 026801 (2006).
 - ⁶ A. S. Blum, J. G. Kushmerick, D. P. Long, C. H. Patterson, J. C. Yang, J. C. Henderson, Y. Yao, J. M. Tour, R. Shashidhar and B. R. Ratna, *Nat Mater* **4**, 167 (2005)
 - ⁷ M. Leijnse and M. R. Wegewijs, *Phys. Rev. B* **78**, 235424 (2008).
 - ⁸ J. Koch and F. von Oppen, *Phys. Rev. Lett.* **94**, 206804 (2005); J. Koch, M. E. Raikh, and F. von Oppen, *Phys. Rev. Lett.* **95**, 056801 (2005); J. Koch, F. von Oppen, and A. V. Andreev, *Phys. Rev. B* **74**, 205438 (2006).
 - ⁹ D. A. Rodrigues, J. Imbers, and A. D. Armour, *Phys. Rev. Lett.* **98**, 067204 (2007).
 - ¹⁰ A. Mitra, I. Aleiner, and A. J. Millis, *Phys. Rev. B* **69**, 245302 (2004).
 - ¹¹ R. P. Feynman and F. L. Vernon, *Annals of Physics* **24**, 118 (1963).
 - ¹² D. Mozyrsky, I. Martin, and M. B. Hastings, *Phys. Rev. Lett.* **92**, 018303 (2004).
 - ¹³ D. Mozyrsky, M. B. Hastings, and I. Martin, *Phys. Rev. B* **73**, 035104 (2006).
 - ¹⁴ M. Brandbyge and P. Hedegård, *Phys. Rev. Lett.* **72**, 2919 (1994).
 - ¹⁵ M. Brandbyge, P. Hedegård, T. F. Heinz, J. A. Misewich, and D. M. Newns, *Phys. Rev. B* **52**, 6042 (1995).
 - ¹⁶ R. Hussein, A. Metelmann, P. Zedler and T. Brandes, *Phys. Rev. B* **82**, 165406 (2010).
 - ¹⁷ S.D. Bennett, J. Maassen and A.A. Clerk, *Phys. Rev. Lett.* **105**, 217206 (2010).
 - ¹⁸ N. Bode, S. V. Kusminskiy, R. Egger and F. von Oppen, *Phys. Rev. Lett.* **107**, 036804 (2011).
 - ¹⁹ A. Nocera, C. A. Perroni, V. Marigliano Ramaglia, and V. Cataudella, *Phys. Rev. B* **83**, 115420 (2011).
 - ²⁰ G. Piovano, F. Cavaliere, E. Paladino and M. Sassetti, *Phys. Rev. B* **83**, 245311 (2011).
 - ²¹ L. S. Schulman, *Techniques and Applications of Path Integration* (Dover Publications, Inc., 2005).
 - ²² U. Weiss, *Quantum Dissipative Systems*, vol. 13 (World Scientific Publishing, 2008).
 - ²³ N. G. Van Kampen, *Stochastic processes in physics and chemistry* (Elsevier, 2008), 3rd ed.
 - ²⁴ H. J. Haug and A.-P. Jauho, *Quantum Kinetics in Transport and Optics of Semiconductors* (Springer-Verlag, 2008), 2nd ed.
 - ²⁵ M. Galperin, M. A. Ratner and A. Nitzan, *Nano Lett.* **5**, 125 (2005).
 - ²⁶ F. Pistolesi, Ya. M. Blanter and I. Martin, *Phys. Rev. B* **78**, 085127 (2008).
 - ²⁷ M. Albert, C. Flindt and M. Büttiker, *Phys. Rev. Lett.* **107**, 086805 (2011).